RSC Advances

PAPER

View Article Online
View Journal | View Issue

Cite this: *RSC Adv.*, 2020, **10**, 24308

Computational study on the mechanisms and kinetics of the CH_2BrO_2 + ClO reaction in the atmosphere†

Yunju Zhang, *[a] Yizhen Tang[b] and Bing He[c]

Received 14th December 2019
Accepted 4th February 2020

DOI: 10.1039/c9ra10511e

rsc.li/rsc-advances

The singlet and triplet potential energy surfaces for the CH_2BrO_2 + ClO reaction are studied at the CCSD(T)/cc-pVTZ//B3LYP/6-311++G(d,p) level. CH_2BrO_2 is revealed to react with ClO through two kinds of mechanisms on the triplet potential energy surface (PES), namely, S_N2 displacement and H-abstraction, and the production of P3 ($CHBrO_2$ + HOCl) *via* H-abstraction is the dominant channel. Addition/elimination and S_N2 displacement mechanisms exist on the singlet PES and are more complicated. The RRKM calculations of the mechanism and product distribution in the CH_2BrO_2 + ClO reaction show that the stabilization of IM1 ($CH_2BrOOOBr$) is dominant at $T \leq 600$ K, while the pathway of producing P1 (CHBrO + HO_2 + Cl) occupies the entire reaction at $T > 600$ K. The total rate constants are independent of pressure, while the individual rate constants are sensitive to pressure. The lifetime of CH_2BrO_2 in the presence of ClO is estimated to be 20.27 h. Moreover, time-dependent density functional theory (TDDFT) calculations suggest that IM1 ($CH_2BrOOOCl$), IM2 ($CH_2BrOOClO$) and IM3 ($CH_2BrOClO_2$) will photolyze under the sunlight.

1. Introduction

Owing to the significant contribution of halogens to stratospheric ozone depletion, the atmospheric oxidation of halogens has been extensively studied in the past decades. In recent years, the oxidation process of halogenated compounds was investigated in the atmosphere because these compounds are conducive to the conversion of halogens in the stratosphere.[1,2] Significant attention has been focused on chlorine compounds, which have a huge impact on the atmosphere. Although the concentration of bromine is very low, it can deplete the stratospheric ozone very effectively; thus, it plays an important role in stratospheric chemistry.[3,4] The oxidation process of brominated compounds has aroused the interest of researchers in recent years. The CH_2Br radical is obtained either by CH_3Br reacting with OH/Cl, which abstracts an H atom from CH_3Br, or the photolysis of C–Br bonds in CH_2Br_2; the CH_2Br radical further reacts with ambient O_2 to produce CH_2BrO_2:[5]

$$CH_3Br + OH/Cl \rightarrow CH_2Br + H_2O/HCl$$

$$CH_2Br \xrightarrow{h\nu} CH_2Br + Br$$

$$CH_2Br + O_2 \rightarrow CH_2BrO_2$$

Because of the significant role of halogens in the stratosphere and troposphere, more and more attention has been focused on them in recent years. For instance, the reactions of ClO with the organic peroxy radicals such as HO_2, CH_3O_2, CF_3O_2, $CFCl_2O_2$ $CFCl_2CH_2O_2$ and CH_3CFClO_2 have been reported experimentally and theoretically.[6–16] However, no studies have been reported for the CH_2BrO_2 + ClO reaction that, in principle, may contribute to the removal of CH_2BrO_2 and ClO and thereby impact stratospheric ozone depletion. Therefore, we first reported the mechanisms of CH_2BrO_2 + ClO, and the possible product channels are presented in Scheme 1. The present theoretical study aims at providing a description of the mechanism and kinetics of the multiple channel reaction and supply data about the gas phase reaction of CH_2BrO_2 + ClO by employing high-level quantum chemical methods and RRKM-TST theory,[17] which has been successfully used with complex reactions.[18–23] In the present kinetic calculations, we used a modified computer program written for the C_2H_5CO + O_2 reaction by Hou and Wang.[19]

[a]*Key Laboratory of Photoinduced Functional Materials, Mianyang Normal University, Mianyang 621000, PR China. E-mail: zhangyj010@nenu.edu.cn; Fax: +86 816 2200819; Tel: +86 816 2200064*

[b]*School of Environmental and Municipal Engineering, Qingdao University of Technology, Fushun Road 11, Qingdao, Shandong, 266033, P. R. China*

[c]*College of Chemistry and Life Science, Institute of Functional Molecules, Chengdu Normal University, Chengdu, Sichuan 611130, PR China*

† Electronic supplementary information (ESI) available. See DOI: 10.1039/c9ra10511e

Scheme 1 The reaction pathways of the CH_2BrO_2 + ClO reaction on the singlet and triplet PESs.

2. Computational methods

2.1 Electronic structure calculations

Full geometry optimizations (including reactants, intermediates, transition states and products) were carried out at the B3LYP[24,25] level of theory using the 6-311++G(d,p) basis set. The B3LYP method has been proven to be an economical and accurate computational model for predicting electronic structures and has been employed widely.[26,27] Compared with other levels of theory, it was found to be sufficiently accurate for predicting the reliable geometries of the stationary points. At the same time, it is not expensive computationally for scanning the potential energy surface. Moreover, B3LYP theory can effectively suppress the problem of spin contaminants. At the same level of geometry optimization, all stationary points were characterized by harmonic vibrational frequency analysis (the number of imaginary frequencies, NIMAG, 0 for minima and 1 for transition state). To confirm that a transition state connects the right reactants and products, the intrinsic reaction coordinate (IRC)[28,29] path was performed at the B3LYP/6-311++G(d,p) level of theory. Based on the B3LYP/6-311++G(d,p) level optimized geometries, the single-point energies of all the species were refined by coupled cluster theory with single and double with perturbative triple excitations CCSD(T)[30] with the cc-pVTZ basis set. To ensure that all stationary points were treated with a single-reference based wave function, the T_1-diagnostic was evaluated for each point using CCSD(T)/cc-pVTZ. The T_1 diagnostic value gives a qualitative assessment of the significance of non-dynamic correction. For closed-shell systems, values exceeding 0.02 are suspect. However, Lee *et al.*[31] suggested that T_1-diagnostic values for open-shell systems may be larger. A number of studies have shown that the multireference wave function is significant if the T_1 diagnostic value calculated is greater than 0.045.[31–34] The T_1 values of the closed-shell and open-shell species in our system are smaller than 0.02 and 0.045, except for TS6, TS13, TS14, T-TS2, and T-TS4. Fortunately, the five species are not important on the triplet and singlet potential energy surfaces and do not affect the reaction mechanism and dynamic behavior. All the calculations were carried out using the GAUSSIAN 09 program package.[35]

2.2 Calculations of rate constants

The microcanonical rate constant was calculated using the RRKM theory as follows:

$$k_i(E) = \alpha_i C_i N_i(E_i^{\neq})/h\rho_j(E_j)$$

In the above equation, α_i is the statistical factor (degeneracy) for the ith reaction path. $N_i(E_i^{\neq})$ is the number of states at the energy above the barrier height for transition state i; $\rho_j(E_j)$ is the density of states at energy E_j of the intermediate. The density of states and the number of states were calculated using the extended Beyer–Swinehart algorithm.[36,37]

3. Results and discussion

The corresponding equilibrium structures of the intermediates and transition states are depicted in Fig. 1, and all the reactants and products are depicted in Fig. 2, with the corresponding limited experimental data.[38] The computational bond lengths of CH_2O, OClO, HOCl, HO_2, ClO, HCl, $O_2(^3\Sigma)$ and O_3 are in good agreement with the corresponding experimental values. To clarify the reaction mechanism, the relevant pathways of the singlet and triplet PESs for the $CHBr_2O_2$ + ClO reaction at the CCSD(T)/cc-pVTZ//B3LYP/6-311++G(d,p) level are depicted in Fig. 3. Table S1† summarizes the

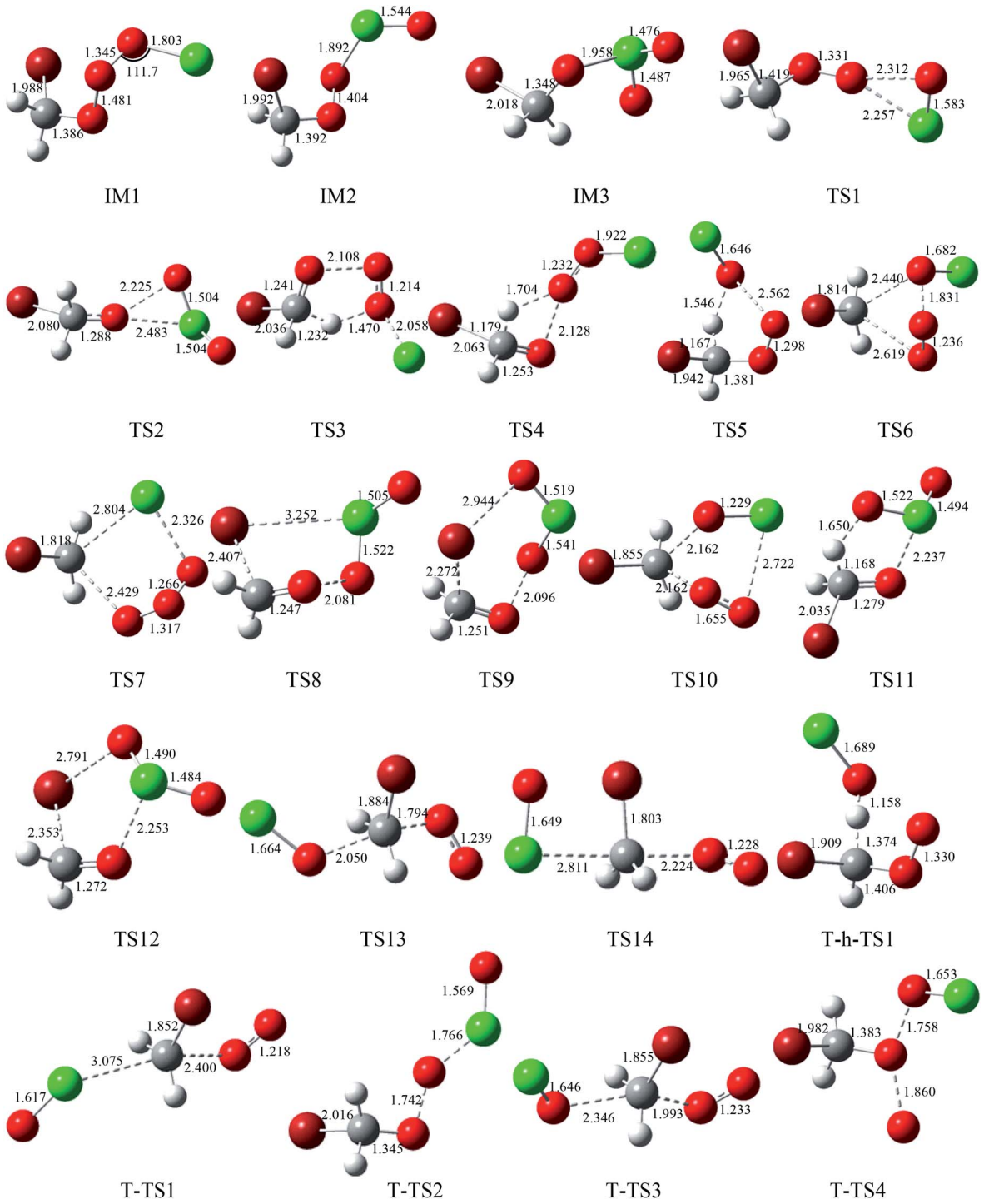

Fig. 1 Optimized geometries (length in Å and angle in degree) for all the intermediates and transition states at the B3LYP/6-311++G(d,p) level.

relative energies including the ZPE corrections of the stationary points. The Z-matrix Cartesian coordinates of all species found on the singlet and triplet PESs are shown in Table S2.† Table S3† displays the harmonic vibrational frequencies and the moment of inertia of all the intermediate and transition states along with available experimental values.

For the title reaction, our results indicate that addition/elimination and S_N2 displacement mechanisms take place on the singlet PES, while S_N2 displacement and H-abstraction mechanisms occur on the triplet PES. Next, we will provide a detailed discussion of these processes.

3.1 The mechanism on the singlet PES

3.1.1 The production of adducts on the singlet PES. On the singlet surface, the most significant characteristic of the

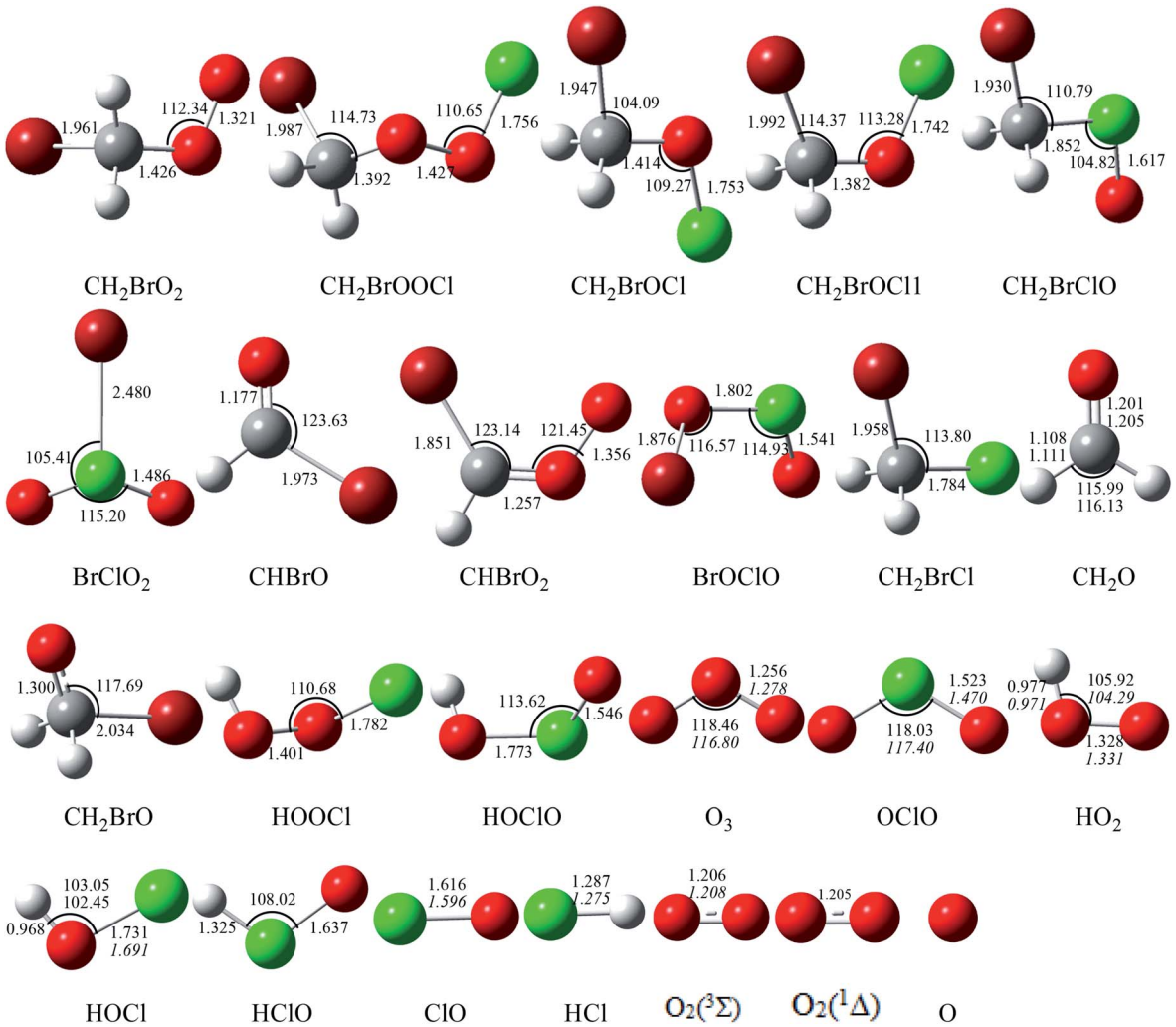

Fig. 2 Optimized geometries (length in Å and angle in degree) for all the reactants and products at the B3LYP/6-311++G(d,p) level. The values in italics are experimental data from ref. 38.

potential energy surface (PES) of the CH_2BrO_2 + ClO reaction is the ability to form the minimum peroxide compound IM1 ($CH_2BrOOOCl$) with no barrier. The newly formed O–O bond is 1.345 Å, the other O–O and C–Br bonds are somewhat longer, and the C–O bond is somewhat smaller than those in the CH_2BrO_2 radical. The isomer IM2 ($CH_2BrOOClO$) is more unstable than IM1 ($CH_2BrOOOCl$) and may be formed passing through the isomerization transition state TS1. TS1 presents a OOCl three-center geometry, which is formed by migration of the Cl atom to the middle-O atom, accompanied with cleavage of the O–O bond. The migrating chlorine is found 2.257 Å away from the shifting end-O by decreasing the OOCl angle from 111.7° to 68.9° and the breaking O–O bond is 2.312 Å. The barrier for IM1 ($CH_2BrOOOCl$) → TS1 → IM2 ($CH_2BrOOClO$) is 28.2 kcal mol^{-1}, and IM2 ($CH_2BrOOClO$) is still 2.2 kcal mol^{-1} higher than the separate molecular CH_2BrO_2 + ClO, so the isomerization process may be possible at high temperatures. Subsequently, IM2 ($CH_2BrOOClO$) can surmount the TS2 barrier, leading to IM3 ($CH_2BrOClO_2$), where the –ClO is transferred to the middle-O atom of the COO– skeleton, and the simultaneous breakage of the O–O bond occurs. The O–O bond breaking in the triangular TS2 is stretched to 2.225 Å and the formed Cl–O bond is 2.483 Å long. The magnitude of the imaginary frequency for TS2 is 140i cm^{-1}. The barrier for the IM2 ($CH_2BrOOClO$) → TS2 → IM3 ($CH_2BrOClO_2$) process is 16.3 kcal mol^{-1}. In any case, the isomerization of IM2 → TS2 → IM3 is energetically more favorable than the isomerization of IM1 → TS1 → IM2 by 11.9 kcal mol^{-1}. Therefore, once IM2 ($CH_2BrOOClO$) is formed, IM1 can easily convert to IM3. At the CCSD(T)//B3LYP level, the energy of IM1 ($CH_2BrOOOCl$), IM2 ($CH_2BrOOClO$) and IM3 ($CH_2BrOClO_2$) are −17.1, 2.2 and −8.0 kcal mol^{-1} relative to CH_2BrO_2 + ClO, respectively, which may involve various dissociation processes, and will be discussed below.

3.1.2 Decomposition channels from IM1 ($CH_2BrOOOCl$) on the singlet PES. The energy-rich addition complex IM1 ($CH_2BrOOOCl$) could decompose to various products. Through TS3, with the 1,4-H shift and the breaking of the O–O bond of the nearly planar HCOOO ring, associated with the breakage of the isolated O–Cl bond (pointed out of the plane), the product

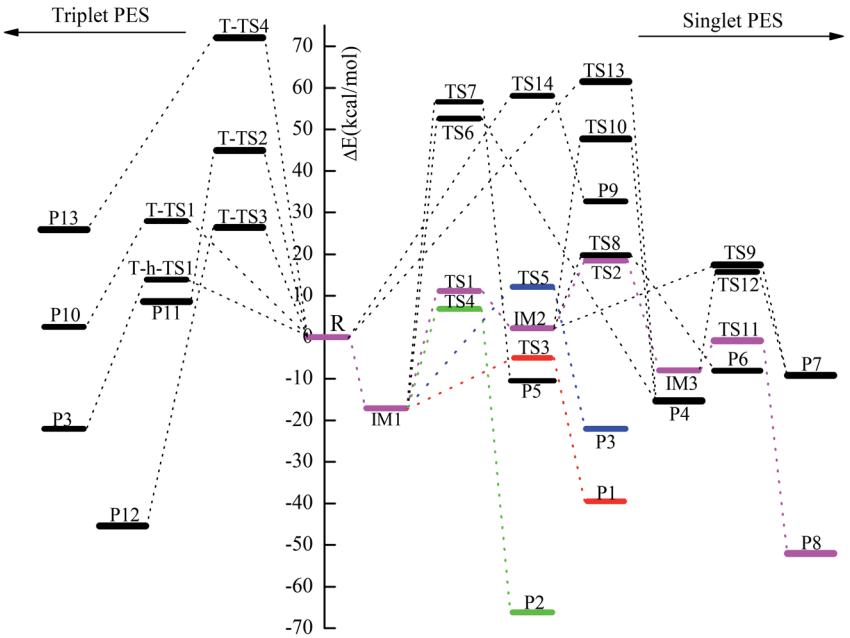

Fig. 3 Potential energy diagram of the reaction channels for the reaction of CH_2BrO_2 with ClO at the CCSD(T)/cc-pVTZ//B3LYP/6-311++G(d,p) level.

P1 (CHBrO + HO_2 + Cl) is formed, which is the most feasible pathway in energy. The barrier for the IM1 → TS3 → P1 process is 12.1 kcal mol^{-1}. The elimination channel is the most exothermic (ΔH = 32.9 kcal mol^{-1}), and the relative Gibbs free energy (ΔG) is −47.5 kcal mol^{-1} (Table S1†), indicating that the decomposition pathway to P1 (CHBrO + HO_2 + Cl) is spontaneous and contributes more to the reaction under certain conditions.

The second route involves the HOOCl-elimination through TS4, with one of the hydrogen atoms in the –CH_2Br group moving to the middle-O atom of the –OOO– skeleton. The breaking C–H and O–O bonds in the HCOO four-center structure TS4 are stretched to 1.179 and 2.128 Å, and the forming O–H bond is 1.704 Å long. Although the whole R (CH_2BrO_2 + ClO) → IM1 ($CH_2BrOOOCl$) → TS4 → P2 (HOOCl + CHBrO) reaction is highly exothermic by about 60.6 kcal mol^{-1}, and the relative Gibbs free energy (ΔG) is −66.7 kcal mol^{-1} (Table S1†), the barrier for the IM1 → TS4 → P2 process is 24.0 kcal mol^{-1}, indicating that this HOOCl-elimination process is spontaneous and may be efficient in the high temperature region.

The production of the P3 ($CHBrO_2$ + HOCl) channel from IM1 ($CH_2BrOOOCl$) takes place *via* an HCOOO five-centered-ring. As shown in Fig. 1, TS5 occurs *via* the migration of one of the hydrogen atoms in the –CH_2Br group to the middle-O atom of the –OOCl skeleton accompanied by cleavage of the O–O bond. In the five-center HCOOO structure, the length of the H atom to either the C atom or the O atom is 1.167 or 1.546 Å, respectively, and the broken O–O bond is 2.562 Å. The IM1 ($CH_2BrOOOCl$) → TS5 → P3 ($CHBrO_2$ + HOCl) reaction is moderately exothermic by 16.4 kcal mol^{-1}, and the HOCl-elimination barrier is predicted to be 29.2 kcal mol^{-1}, which are 17.1 and 5.2 kcal mol^{-1} higher than the processes of IM1 → TS3 → P1 and IM1 → TS4 → P2, respectively, suggesting that the HOCl-elimination pathway is less competitive with the production of the P1 (CHBrO + HO_2 + Cl) and P2 (HOOCl + CHBrO) pathways, and may be unimportant for the CH_2BrO_2 + ClO reaction.

In addition, the –ClO group or Cl atom shifting from IM1 ($CH_2BrOOOCl$) respectively undergoes the COOO four-center transition state TS6 or COOOCl five-center transition state TS7 to produce P4 ($CH_2BrOCl + O_2(^1\Delta_g)$) and P5 ($CH_2BrCl + O_3$). In TS6, the C–O and O–O bonds that will be broken and the C–O bond that will be formed are extremely long at 2.619, 1.831, and 2.440 Å, respectively. In TS7, the breaking C–O and O–Cl bonds and the forming C–Cl bond are 2.429, 2.326, and 2.804 Å, respectively. The vibrational frequency analysis of TS6 and TS7 suggest only one imaginary frequency of 378i and 461i cm^{-1}, respectively. The energy barriers for the dissociation of IM1 ($CH_2BrOOOCl$) → TS6 → P4 ($CH_2BrOCl + O_2$ ($^1\Delta_g$)) and IM1 ($CH_2BrOOOCl$) → TS7 → P5 ($CH_2BrCl + O_3$) are extremely high, 69.7 and 73.7 kcal mol^{-1}, respectively, and thus these two dissociation channels may be excluded judging from the higher barrier heights.

3.1.3 Decomposition channels from IM2 ($CH_2BrOOClO$) on the singlet PES. When we considered the decomposition channels from IM2 ($CH_2BrOOClO$), it could undergo respective O–O bond breaking associated with the 1,4-Br shift or 1,5-Br shift from the C to the Cl atom or the terminal-O atom of the –OClO skeleton (*i.e.*, TS8 and TS9) to yield the final product P6 (CH_2O + $BrClO_2$) and P7 (CH_2O + BrOClO). In TS8 and TS9, the loose COOClBr five-membered ring and COOClOBr six-membered ring are non-planar, respectively. In TS8, the Cl–Br bond that will be formed and the C–Br and O–O bonds that will be broken are as long as 3.252, 2.407, and 2.081 Å, respectively.

In TS9, the breaking O–O and C–Br bonds and the forming Br–O bond are 2.096, 2.272, and 2.944 Å, respectively. The barrier heights for the channels of IM2 ($CH_2BrOOClO$) → TS8 → P6 ($CH_2O + BrClO_2$) and IM2 ($CH_2BrOOClO$) → TS9 → P7 (CH_2O + BrOClO) are 17.6 and 15.2 kcal mol^{-1}, which are 1.3 kcal mol^{-1} higher and 1.1 kcal mol^{-1} lower than the process of IM2 → TS2 → IM3, suggesting that these three channels could be competitive with each other.

P4 ($CH_2BrOCl + O_2(^1\Delta_g)$) could also be produced from IM2 ($CH_2BrOOClO$) *via* transition state TS10 involving the terminal-O atom migrating to the carbon atom, associated with the C–O and Cl–O bonds breaking. The located loose COOClO five-centered-ring is non-planar in TS10. In comparison with the production channels of P6 ($CH_2O + BrClO_2$) and P7 (CH_2O + BrOClO) from IM2 ($CH_2BrOOClO$), the pathway of IM2 (CH_2-BrOOClO) → TS10 → P4 ($CH_2BrOCl + O_2$) has a higher dissociation barrier (45.6 kcal mol^{-1}), meaning this decomposition pathway may not be plausible for the title reaction.

3.1.4 Decomposition channels from IM3 ($CH_2BrOClO_2$) on the singlet PES. Two possible decomposition channels from IM3 ($CH_2BrOClO_2$) are the elimination of the HOClO or BrOClO to form CHBrO or CH_2O, respective with either the H atom or Br atom in the –CH_2Br group shifting to the O atom, associated with the O–Cl bond cleavage. The BrOClO-elimination is not important compared with the HOClO-eliminations, as the BrOClO-elimination barrier is 16.6 kcal mol^{-1} higher than the HOClO-elimination. Moreover, the overall exothermicity of the IM3 → TS11 → P8 (CHBrO + HOClO) and IM3 → TS12 → P7 (CH_2O + BrOClO) reactions are 46.3 and 3.0 kcal mol^{-1}, implying that P8 (CHBrO + HOClO) is easily produced once IM3 ($CH_2BrOClO_2$) is produced.

3.1.5 S_N2 displacement channels on the singlet PES. The O atom or the Cl atom in the ClO radical could attack the C site of CH_2BrO_2, kicking off the O_2 ($^1\Delta_g$) and producing the CH_2BrOCl or CH_2BrClO, respectively. The transition states involved in these two substitution steps are TS13 and TS14, respectively. The forming and breaking C–O bond in TS13 are 2.050 and 1.794 Å, meanwhile the forming C–Cl bond and breaking C–O bond in TS14 are 2.811 and 2.224 Å, respectively. The barrier heights for these two channels, 61.5 and 58.1 kcal mol^{-1}, are rather high, therefore, these two elementary substitution channels are prohibited for the title reaction.

3.2 The mechanisms on the triplet PES

H-abstraction and S_N2 displacement reaction mechanisms are presented on the triplet surface. The P3 ($CHBrO_2$ + HOCl) products on the triplet PES, exothermic by 16.4 kcal mol^{-1}, can be achieved by the O atom of the ClO radical directly abstracting from the –CH_2Br group through T-h-TS1. The barrier of CH_2BrO_2 + ClO → T-h-TS1 → P3 ($CHBrO_2$ + HOCl) is 13.9 kcal mol^{-1}, which involves the lowest barrier on the PES. Four S_N2 displacement reaction channels between CH_2BrO_2 and ClO could take place on the triplet PES. The Cl atom of the ClO radical could attack the carbon atom or the terminal oxygen atom of the CH_2BrO_2, kicking off the O_2 ($^3\Sigma$) or CH_2BrO to give CH_2BrClO or OClO *via* T-TS1 or T-TS2, or the oxygen atom of the ClO radical could attack the carbon atom or the middle oxygen atom of the CH_2BrO_2, simultaneously with the departure of $O_2(^3\Sigma)$ and $O(^3P)$, leading to CH_2BrOCl or CH_2-BrOOCl *via* T-TS3 or T-TS4, respectively. The predicted heat of reaction for the production of P10 ($CH_2BrClO + O_2(^3\Sigma)$), P11 ($CH_2BrO$ + OClO), P12 ($CH_2BrOCl + O_2(^3\Sigma)$) and P13 ($CH_2$-BrOOCl + $O(^3P)$) is 8.5, 14.1, −39.6 and 31.7 kcal mol^{-1}, respectively. The above four substituent channels involve high barriers (28.0, 45.0, 26.4 and 72.0 kcal mol^{-1}) with respect to the reactants, which are 14.1, 31.1, 12.5 and 58.1 kcal mol^{-1} higher than that of the H-abstraction pathway, thus, these four substituent routes on the triplet are not competitive with the H-abstraction pathway.

3.3 Rate constant calculations

As discussed above, for the reaction pathways producing P1, P2, P3, P6, P7 and P8 (Scheme 1), the reaction energy barriers are lower and the reactions are exothermic, so these reaction pathways are involved in the kinetics calculations. However, the reaction pathways producing P4, P5, P9, P10, P11, P12 and P13 with higher energy barriers are less competitive in energy, and their contribution to the total reaction is negligible.

Temperature- or pressure-dependent rate constants for the important pathways (Scheme 2) of the CH_2BrO_2 + ClO reaction were calculated at 200–3000 K and 10^{-10} to 10^{10} atm using RRKM theory, based on the optimized geometries, moment of inertia and frequencies obtained at the B3LYP/6-311++G(d,p) level, and the energies were obtained at the CCSD(T)/cc-pVTZ level.

The steady-state approximation for all energized intermediates (IM1*, IM2* and IM3*) leads to the following expressions:

$$k_{IM1}(T,P) = \frac{\alpha_a}{h}\frac{Q_t^{\neq}Q_r^{\neq}}{Q_{CH_2BrO_2}Q_{ClO}}e^{-E_a/RT} \times \int_0^{\infty}\frac{\omega}{X_3}N_a(E^{\neq})e^{-E^{\neq}/RT}dE^{\neq} \quad (1)$$

$$k_{IM2}(T,P) = \frac{\alpha_a}{h}\frac{Q_t^{\neq}Q_r^{\neq}}{Q_{CH_2BrO_2}Q_{ClO}}e^{-E_a/RT} \times \int_0^{\infty}\frac{\omega X_2}{X_3}N_a(E^{\neq})e^{-E^{\neq}/RT}dE^{\neq} \quad (2)$$

$$k_{IM3}(T,P) = \frac{\alpha_a}{h}\frac{Q_t^{\neq}Q_r^{\neq}}{Q_{CH_2BrO_2}Q_{ClO}}e^{-E_a/RT} \times \int_0^{\infty}\frac{\omega X_1 X_2}{X_3}N_a(E^{\neq})e^{-E^{\neq}/RT}dE^{\neq} \quad (3)$$

$$k_{P1}(T,P) = \frac{\alpha_a}{h}\frac{Q_t^{\neq}Q_r^{\neq}}{Q_{CH_2BrO_2}Q_{ClO}}e^{-E_a/RT} \times \int_0^{\infty}\frac{k_2(E)}{X_3}N_a(E^{\neq})e^{-E^{\neq}/RT}dE^{\neq} \quad (4)$$

$$k_{P2}(T,P) = \frac{\alpha_a}{h}\frac{Q_t^{\neq}Q_r^{\neq}}{Q_{CH_2BrO_2}Q_{ClO}}e^{-E_a/RT} \times \int_0^{\infty}\frac{k_3(E)}{X_3}N_a(E^{\neq})e^{-E^{\neq}/RT}dE^{\neq} \quad (5)$$

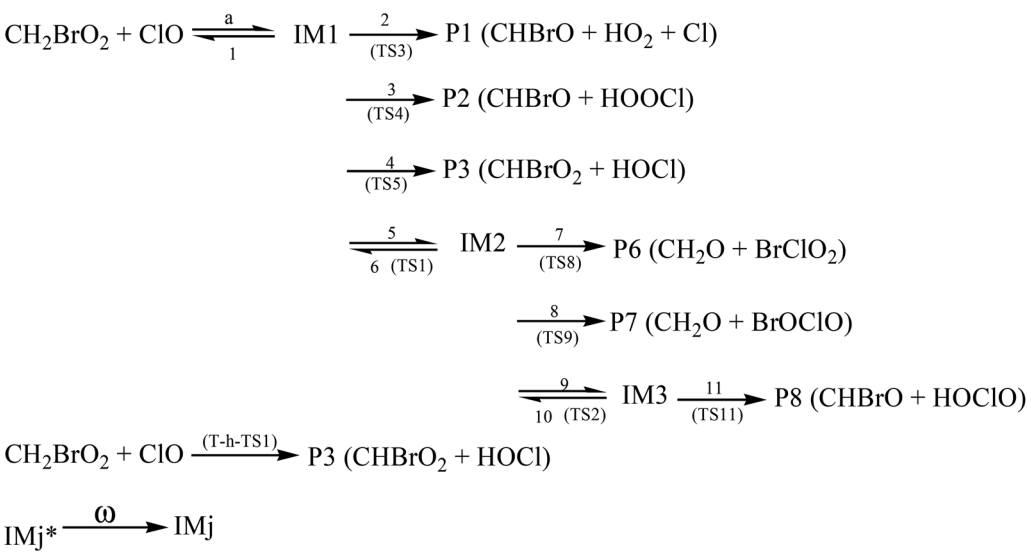

Scheme 2 The dominant channels for the CH_2BrO_2 + ClO reaction.

$$k_{P3}(T,P) = \frac{\alpha_a}{h}\frac{Q_t^{\neq}Q_r^{\neq}}{Q_{CH_2BrO_2}Q_{ClO}}e^{-E_a/RT} \times \int_0^{\infty}\frac{k_4(E)}{X_3}N_a(E^{\neq})e^{-E^{\neq}/RT}dE^{\neq} \quad (6)$$

$$k_{P6}(T,P) = \frac{\alpha_a}{h}\frac{Q_t^{\neq}Q_r^{\neq}}{Q_{CH_2BrO_2}Q_{ClO}}e^{-E_a/RT} \times \int_0^{\infty}\frac{k_7(E)X_2}{X_3}N_a(E^{\neq})e^{-E^{\neq}/RT}dE^{\neq} \quad (7)$$

$$k_{P7}(T,P) = \frac{\alpha_a}{h}\frac{Q_t^{\neq}Q_r^{\neq}}{Q_{CH_2BrO_2}Q_{ClO}}e^{-E_a/RT} \times \int_0^{\infty}\frac{k_8(E)X_2}{X_3}N_a(E^{\neq})e^{-E^{\neq}/RT}dE^{\neq} \quad (8)$$

$$k_{P8}(T,P) = \frac{\alpha_a}{h}\frac{Q_t^{\neq}Q_r^{\neq}}{Q_{CH_2BrO_2}Q_{ClO}}e^{-E_a/RT} \times \int_0^{\infty}\frac{k_{11}(E)X_1X_2}{X_3}N_a(E^{\neq})e^{-E^{\neq}/RT}dE^{\neq} \quad (9)$$

with the following definitions:

$$X_1 = k_9(E)/(k_{10}(E) + k_{11}(E) + \omega)$$

$$X_2 = k_5(E)/(k_6(E) + k_7(E) + k_8(E) + k_9(E) + \omega - k_{10}(E)X_1)$$

$$X_3 = k_1(E) + k_2(E) + k_3(E) + k_4(E) + k_5(E) + \omega - k_6(E)X_2$$

In the above equations, α_a is the statistical factor for the reaction path a, and E_a is the energy barrier for the reaction step a. Q_{ClO} and $Q_{CH_2BrO_2}$ are the total partition functions of ClO and CH_2BrO_2, respectively; $Q_t^{\neq}$ and $Q_r^{\neq}$ are the translational and rotational partition functions of the entrance transition state, respectively; $N_a(E^{\neq})$ is the number of states for the association transition state with excess energy $E^{\neq}$ above the association barrier. $k_i(E)$ is the energy-specific rate constant for the ith channel and C_i is the ratio of the overall rotational partition function of the TS_i and IM_j.

Based on the above thermodynamic results obtained at the CCSD(T)//B3LYP level, the kinetic calculations were performed for the dominant addition/elimination channels (on the singlet PES) and the direct H-abstraction channel (on the triplet PES) using RRKM theory. The temperature dependence of the total and individual rate constants at a selected temperature range of 200–3000 K are shown in Fig. 4. The rate constants for IM1 ($CH_2BrOOOCl$), IM2 ($CH_2BrOOClO$), IM3 ($CH_2BrOClO_2$), P1 (CHBrO + HO_2 + Cl), P2 (CHBrO + HOOCl), P3 ($CHBrO_2$ + HOCl), P6 (CH_2O + $BrClO_2$), P7 (CH_2O + BrOClO), and P8 (CHBrO + HOClO) and the rate constants of the H-abstraction channel on the triplet PES are labeled as k_{IM1}, k_{IM2}, k_{IM3}, k_{P1}, k_{P2}, k_{P3}, k_{P6}, k_{P7}, k_{P8} and $k_{T\text{-}h\text{-}TS1}$, respectively. The overall rate constant for the CH_2BrO_2 + ClO reaction is denoted as k_{over}, where $k_{over} = k_{IM1} + k_{IM2} + k_{IM3} + k_{P1} + k_{P2} + k_{P3} + k_{P6} + k_{P7} + k_{P8} + k_{T\text{-}h\text{-}TS1}$.

Fig. 4 reveals the contributions of IM1, IM2, IM3, P1, P2, P3, P6, P7, P8 and the H-abstraction channel on the triplet PES to the CH_2BrO + ClO reaction *versus* 1000/T between 200 and 3000 K. Fig. 4 indicates that k_{IM1} reveals weak temperature dependence at $T \leq 600$ K first and then decreases with increasing temperature, and the rate constants for other pathways exhibit a positive temperature dependence at 200–3000 K. The contribution of IM1 ($CH_2BrOOOCl$) takes over the reaction below 600 K. Meanwhile, the contribution of P1 (CHBrO + HO_2 + Cl) becomes more important than that of other products at $T >$ 600 K. For example, the values of k_{IM1}/k_{over} are 1.00 at 200 K and 0.62 at 600 K (Fig. 5), respectively. However, as the temperature increases, the channel of production of P1 (CHBrO + HO_2 + Cl) overcomes IM1 ($CH_2BrOOOCl$) and becomes predominant, and the ratios of k_{P1}/k_{over} are 0.56 at 600 K, 0.94 at 1400 K and 0.66 at 3000 K (Fig. 5).

RRKM calculated the overall high-pressure limit rate constants $k_{inf(over)}$ and the individual high-pressure limit rate

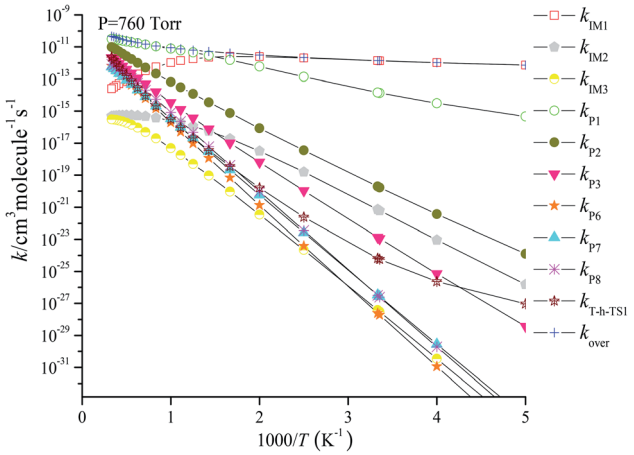

Fig. 4 Predicted rate coefficients of total and individual primary pathways at 760 torr, N_2 in the temperature region of 200–3000 K for the CH_2BrO_2 + ClO reaction.

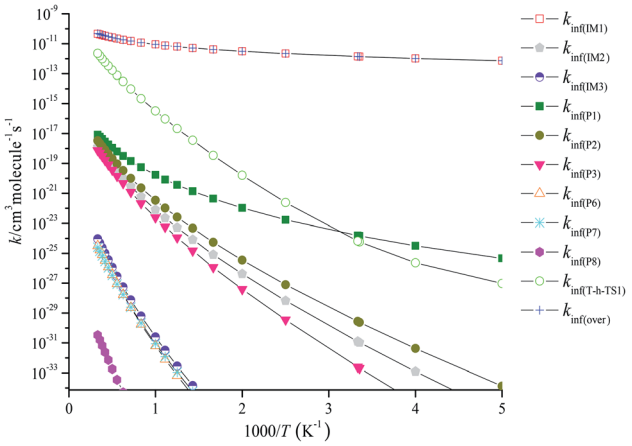

Fig. 6 Predicted high-pressure limit rate coefficients of total and individual primary pathways at high pressure in the temperature region of 200–3000 K.

constants $k_{inf(IM1)}$, $k_{inf(IM2)}$, $k_{inf(IM3)}$, $k_{inf(P1)}$, $k_{inf(P2)}$, $k_{inf(P3)}$, $k_{inf(P6)}$, $k_{inf(P7)}$, $k_{inf(P8)}$ and $k_{inf(T\text{-}h\text{-}TS1)}$ in the temperature range of 200–3000 K are illustrated in Fig. 6. $k_{inf(IM1)}$ is equal to $k_{inf(over)}$, which implies that the most favorable channel is the stabilization of IM1 ($CH_2BrOOOCl$) at 200–3000 K. For the main emphasis is on atmospheric applications, the three-parameter Arrhenius fits the total high-pressure limit rate constants $k_{inf(over)}$ (in units of cm^3 per molecule per s) within 200–3000 K as follows:

$$k_{inf(over)} = 2.20 \times 10^{-16} T^{1.54} \exp(-0.54/T) (200 \leq T \leq 3000\ \text{K})$$

We also investigated the pressure effect of the total and branching reaction rate constants at selected temperatures of 298, 500, 1000 and 3000 K (Fig. 7) and a pressure range of 10^{-10} to 10^{10} torr. Obviously, the overall rate constants are not subject to pressure. At 298, 500, 1000 and 3000 K, the stabilization of the IM1 ($CH_2BrOOOCl$) is the significant channel at $P \geq 10^1$, $P \geq 10^2$, $P \geq 10^4$ and $P \geq 10^6$ torr, respectively; at lower pressure, the production of P1 (CHBrO + HO_2 + Cl) is the dominant reaction channel.

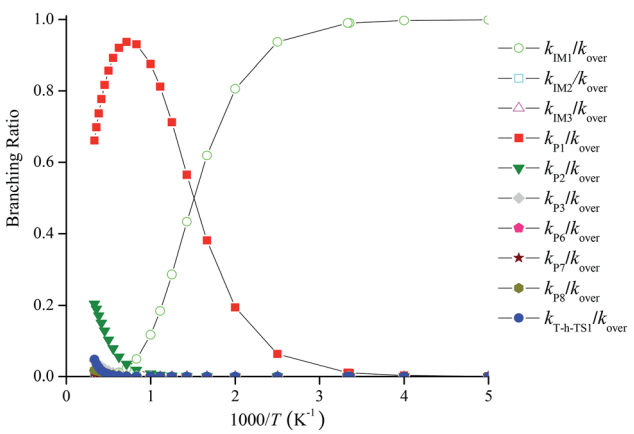

Fig. 5 Forecasted branching ratios for the CH_2BrO_2 + ClO reaction at 760 torr.

3.4 Vertical excitation energy of IM1 ($CH_2BrOOOCl$), IM2 ($CH_2BrOOClO$) and IM3 ($CH_2BrOClO_2$)

The photo-oxidation of compounds containing bromine and chlorine is significant for Br and Cl atmospheric chemistry, which as sources of Br and Cl, the photolysis might affect the stratosphere and troposphere. To gain new insights into the photolytic stability of the Br and Cl containing compounds, the vertical excitation energy (T_V) of the first ten excited states for IM1 ($CH_2BrOOOCl$), IM2 ($CH_2BrOOClO$) and IM3 ($CH_2BrOClO_2$) were calculated by the TDDFT method using B3LYP/6-311++G(d,p), and the results comprising wavelength (λ), excitation energy (T_V) and oscillator strength (f) are listed in Table 1. Compounds will be considered to photolyze if the T_V value is smaller than 4.1 eV or the wavelength is longer than 300 nm.[39,40] From Table 1, it is seen that the T_V value of the first three excited states of IM1 ($CH_2BrOOOCl$) and IM3 ($CH_2BrOClO_2$) are 382 nm (3.2 eV), 340 nm (3.6 eV), and 329 nm (3.7 eV) and 482 nm (2.5 eV), 465 nm (2.6 eV), and 410 nm (3.0 eV), respectively, and their oscillator strengths are 0.0014, 0.0003, and 0.0168, and 0.0021, 0.0202, and 0.0035. The first four excited states of IM2 ($CH_2BrOOClO$) are 684 nm (1.8 eV), 374 nm (3.3 eV), 364 nm (3.4 eV) and 331 nm (3.7 eV), and the oscillator strengths are 0.0001, 0.0082, 0.0075, and 0.0041, respectively, indicating the possibility of photolysis of IM1 ($CH_2BrOOOCl$), IM2 ($CH_2BrOOClO$) and IM3 ($CH_2BrOClO_2$) under sunlight, which will cause them to be an origin of reactive bromine and chlorine species in the atmosphere.

3.5 Atmospheric lifetime of CH_2BrO_2

The atmospheric lifetime of CH_2BrO_2 can be calculated using the following formula: $\tau = \frac{1}{k[ClO]}$. Using the total rate constants, 1.37×10^{-12} cm^3 per molecule per s for the CH_2BrO_2 + ClO reaction at 298 K and the global atmospheric ClO

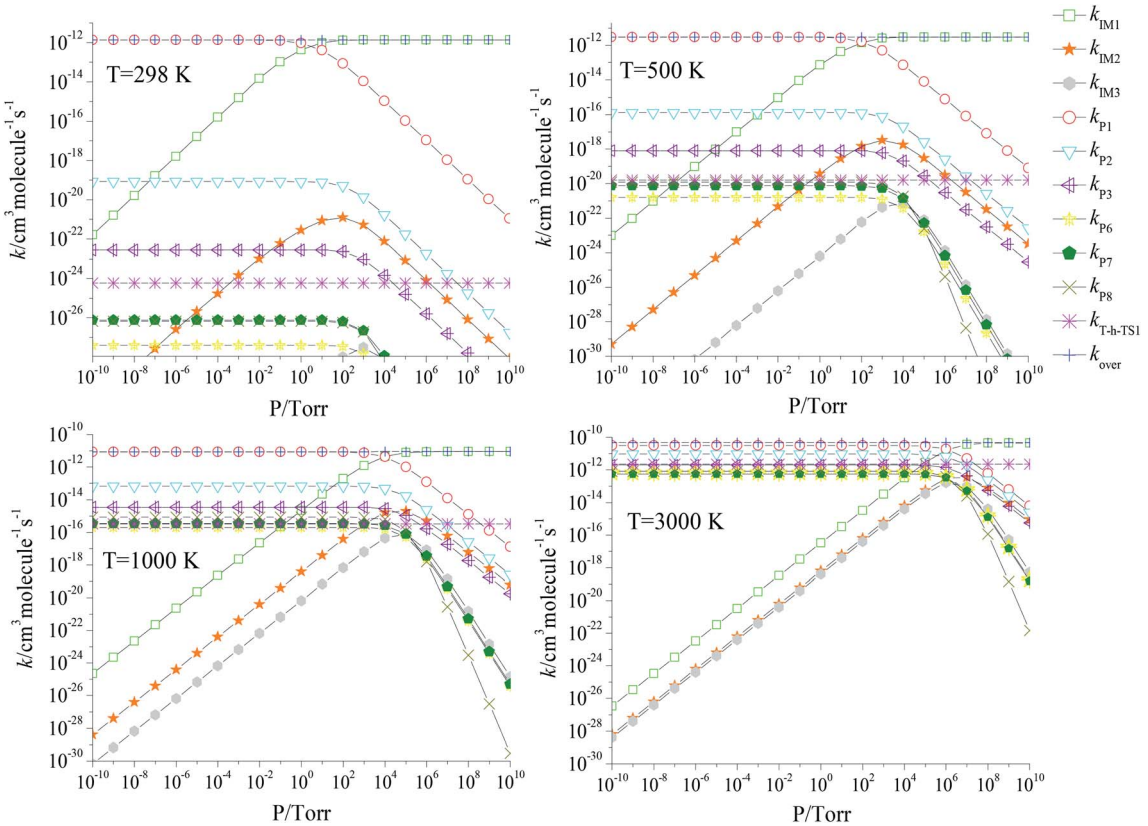

Fig. 7 Predicted rate coefficients of total and individual primary pathways at high pressures in the temperature region of 200–3000 K.

concentrations 1×10^7 molecules per cm^3,[41] the lifetime of CH_2BrO_2 was estimated to be 20.27 h, which suggests that the reaction of CH_2BrO_2 + ClO plays an important role in some special areas and the marine boundary layer.

3.6 Atmospheric implications of CHBrO

With the concentration of around 10^7 molecules per cm^3 in the stratosphere, OH/ClO radicals play a significant role in the degradation processes of many molecules.[42] Thus, the formation of CHBrO as a major product in the title reaction could lead to further reactions with OH and ClO, respectively. To be thorough, the CHBrO + ClO/OH reactions were studied by the same methods, and the corresponding PESs are depicted in Fig. 8a and b, as well. According to the calculations, two channels were located *via* different transition states for these two reactions. The first scenario starts from transition states TS-ClO or TS-OH surmounting the barrier of 16.55 or 8.00 kcal mol^{-1}, leading to the final products HCOOCl + Br or HCOOH + Br, respectively. Moreover, the hydrogen atom in CHBrO could be abstracted by OH/ClO radicals *via* h-TS-ClO or h-TS-OH. The IRC calculation

Table 1 The excitation energy T_V (in eV), oscillator strength f (in atomic units) and wavelength λ (in nm) of the first five excited states of IM1 ($CH_2BrOOOCl$), IM2 (CH_2BrO_2ClO) and IM3 ($CH_2BrOClO_2$) at the TD-B3LYP/6-311++(d,p) level of theory

	IM1 ($CH_2BrOOOCl$)			IM2 ($CH_2BrOOClO$)			IM3 ($CH_2BrOClO_2$)		
Excited states	T_V	F	λ	T_V	f	λ	T_V	f	λ
1	3.2	0.0014	382.37	1.8	0.0001	684.81	2.5	0.0021	482.56
2	3.6	0.0003	340.18	3.3	0.0082	374.45	2.6	0.0202	465.33
3	3.7	0.0168	329.99	3.4	0.0075	364.59	3.0	0.0035	410.05
4	4.2	0.0003	294.26	3.7	0.0041	331.18	4.1	0.0518	299.90
5	4.4	0.0095	277.97	4.2	0.1482	289.55	4.3	0.0018	286.12
6	5.1	0.0037	239.07	4.8	0.0014	253.87	5.4	0.2292	229.05
7	5.2	0.0199	234.54	5.4	0.0297	226.09	5.4	0.0293	226.33
8	5.45	0.0592	227.54	5.6	0.0049	217.93	5.6	0.0007	219.90
9	5.6	0.0084	220.97	5.8	0.0002	211.35	5.8	0.0018	212.98
10	5.6	0.0882	218.85	6.1	0.0077	202.31	5.9	0.0013	206.78

confirms that the corresponding product is BrCO + HOCl or BrCO + H_2O. The barrier height of h-TS-ClO and h-TS-OH is about 25.46 and −1.36 kcal mol^{-1}. Thus, the OH-initiated reaction might be one of the main removal pathways for CHBrO.

3.7 Comparisons with the similar reaction of CH_3O_2 + ClO

In order to gain a deeper understanding of the reaction of CH_2BrO_2 + ClO, it is very important to compare the mechanism and kinetics between the title reaction and a similar system (CH_3O_2 + ClO).[43] It is concluded that the addition/elimination and S_N2 displacement mechanisms are found both on the singlet PES of the above two reactions. On the triplet PES, H-abstraction and S_N2 displacement mechanisms are found for the CH_2BrO_2 + ClO reaction and only addition/elimination is identified for the CH_3O_2 + ClO reaction. By comparing the two reactions, we find that the most favorable channel is the oxygen atom in ClO attacking the terminal-O atom in CH_2BrO_2 and CH_3O_2, forming the intermediate $CH_2BrOOOCl$ and CH_3OOOCl, and then decomposition to the final products CHBrO + HO_2 + Cl and CH_2O + HOOCl. The Br-substituted effect could be speculated to be of no significant role in the reactions of CH_2BrO_2 and CH_3O_2 with ClO in the atmospheric conditions. Also, no kinetic behaviors were discovered for the CH_3O_2 + ClO reaction theoretically. The total rate constants show temperature dependence and pressure independence for the reaction between CH_2BrO_2 and ClO.

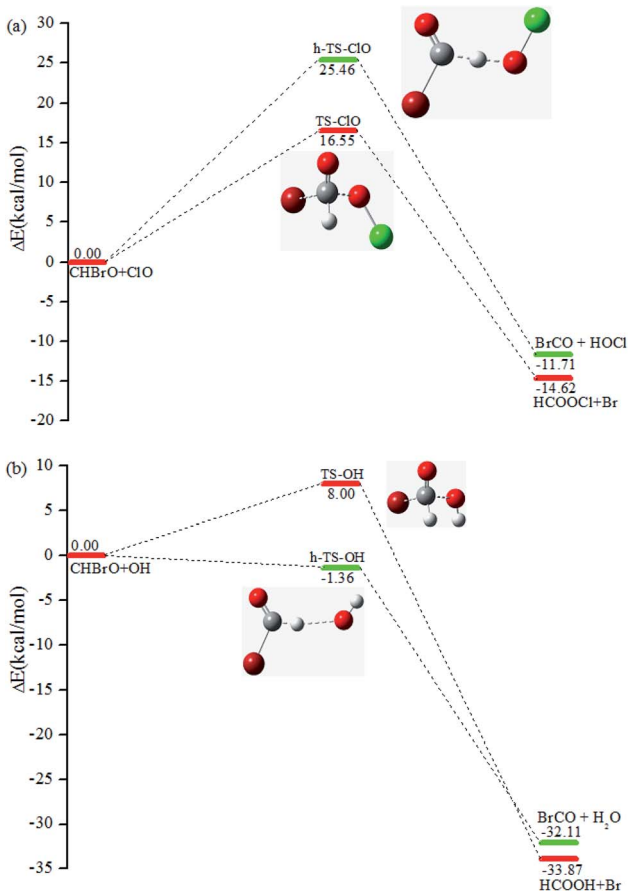

Fig. 8 Reaction channels and relative energy (unit: kcal mol^{-1}) at the CCSD(T)/cc-pVTZ//B3LYP/6-311++G(d,p) level. (a) The energetic profile of the CHBrO with ClO reaction. (b) The energetic profile of the CHBrO with OH reaction.

4. Conclusions

The atmospheric oxidation process of CH_2BrO + ClO was studied at the CCSD(T)//B3LYP level of theory. H-abstraction and S_N2 displacement mechanisms on the triplet PES, and addition/elimination and S_N2 displacement mechanisms on the singlet PES were identified, respectively. The dominant reaction mechanism on the triplet PES is H-abstraction, and on the singlet PES, addition/elimination. The rate constants of the title reaction at 200–3000 K have been calculated employing a Fortran code based on RRKM theory. According to the obtained kinetics data, the ClO-addition to the terminal-O of CH_2BrO_2 producing IM1 ($CH_2BrOOOCl$) dominates the title reactions at $T \geq 600$ K on the singlet PES, and the O atom of ClO abstracting one of the H atoms in CH_2BrO_2 dominates the whole reaction at $T > 600$ K on the triplet PES. The atmospheric lifetime of CH_2BrO_2 in the presence of ClO is predicted to be 20.27 h. IM1 ($CH_2BrOOOCl$), IM2 ($CH_2BrOOClO$) and IM3 ($CH_2BrOClO_2$) will photolyze under sunlight, which might be one source of Br and Cl containing species in the atmosphere.

Conflicts of interest

There are no conflicts to declare.

Acknowledgements

This work was supported by the Natural Science Foundations of China (No. 21707062 & 41775119), Scientific Research Starting Foundation of Mianyang Normal University (No. QD2016A007).

References

1 B. Finlayson-Pitts and J. N. Pitts Jr, *Chemistry of the Upper and Lower Atmosphere*, Academic Press, New York, 1999.
2 R. P. Wayne, *Chemistry of Atmospheres*, Oxford University Press, Oxford, 3rd edn, 2000.
3 D. L. Albritton and R. T. Watson, *Methyl Bromide: Its Atmospheric Science, Technology and Economics, Montreal Protocol Assessment Supplement*. UNEP, Nairobi, Kenya, 1993.
4 S. A. Montzka and S. Reimann, *et al.*, Ozone-depleting substances (ODSs) and related chemicals. Scientific Assessment of Ozone Depletion: 2010, *Global Ozone Research and Monitoring Project Report No. 52*, World Meteorological Organization, Geneva, Switzerland, ch. 1, 2011.
5 W. S. McGivern, H. Kim, J. S. Francisco and S. W. North, *J. Phys. Chem. A*, 2004, **108**, 7247–7252.
6 K. M. Hickson, L. F. Keyser and S. P. Sander, *J. Phys. Chem. A*, 2007, **111**, 8126–8138.

7 S. L. Nickolaisen, S. M. Roehl, L. K. Blakely, R. R. Fridel, J. S. Francisco, R. F. Liu and S. P. Sander, *J. Phys. Chem. A*, 2000, **104**, 308–319.
8 G. P. Knight, T. Beiderhase, F. Helleis, G. K. Moortgat and J. N. Crowley, *J. Phys. Chem. A*, 2000, **104**, 1674–1685.
9 Z. F. Xu, R. S. Zhu and M. C. Lin, *J. Phys. Chem. A*, 2003, **107**, 3841–3850.
10 E. Drougas, A. F. Jalbout and A. M. Kosmas, *J. Phys. Chem. A*, 2003, **107**, 11386–11390.
11 F. Helleis, J. N. Crowley and G. K. Moortgat, *J. Phys. Chem.*, 1993, **97**, 11464–11473.
12 F. Helleis, J. N. Crowley and G. K. Moortgat, *Geophys. Res. Lett.*, 1994, **21**, 1795–1798.
13 A. S. Kukui, T. P. W. Jungkamp and R. N. Schindler, *Ber. Bunsen Phys Chem.*, 1994, **98**, 1298–1302.
14 Y. Z. Tang, H. F. Sun, J. Y. Sun, Y. J. Zhang and R. S. Wang, *Atmos. Environ.*, 2014, **92**, 367–375.
15 A. Horowitz, G. Schuster and G. K. Moortgat, *Int. J. Chem. Kinet.*, 1992, **24**, 255–269.
16 F. X. Wu and R. W. Carr, *J. Phys. Chem.*, 1995, **99**, 3128–3136.
17 K. A. Holbrook, M. J. Pilling and S. H. Robertson, *Unimolecular Reactions*, J. Wiley, Chichester, UK, 1996.
18 H. Hou, B. S. Wang and Y. S. Gu, *J. Phys. Chem. A*, 2000, **104**, 320–328.
19 H. Hou and B. S. Wang, *J. Chem. Phys.*, 2007, **127**, 054306.
20 J. A. Manion and I. A. Awan, *Int. J. Chem. Kinet.*, 2018, **50**, 225–242.
21 Y. Z. Tang, C. G. Lu, J. Y. Sun, *et al*, *Environ. Sci. Pollut. Res.*, 2019, **26**, 2345–2352.
22 S. H. Mousavipour, S. Ramazani and Z. Shahkolahi, *J. Phys. Chem. A*, 2009, **113**, 2838.
23 Y. J. Zhang, J. Y. Sun, W. Q. Zhang, Y. Z. Tang and R. S. Wang, *J. Comput. Chem.*, 2014, **35**, 1646–1656.
24 A. D. Becke, *J. Chem. Phys.*, 1993, **98**, 5648.
25 C. Lee, W. Yang and R. G. Parr, *Phys. Rev. B*, 1988, **37**, 785.
26 J. Zhao and R. Y. Zhang, *Atmos. Environ.*, 2008, **42**, 5849–5858.
27 Y. Z. Tang and C. J. Nielsen, *Atmos. Environ.*, 2012, **55**, 185–189.
28 C. Gonzalez and H. B. Schlegel, *J. Chem. Phys.*, 1989, **90**, 2154–2161.
29 C. Gonzalez and H. B. Schlegel, *J. Phys. Chem.*, 1990, **94**, 5523–5527.
30 K. Raghavachari, G. W. Trucks, J. A. Pople and M. Head-Gordon, *Chem. Phys. Lett.*, 1989, **157**, 479–483.
31 T. J. Lee and P. R. Taylor, *Int. J. Quantum Chem.*, 1989, **23**, 199.
32 J. Peiró-García and I. Nebot-Gil, *ChemPhysChem*, 2003, **4**, 843.
33 J. Peiró-García and I. Nebot-Gil, *J. Comput. Chem.*, 2003, **24**, 1657.
34 J. C. Rienstra-Kiracofe, W. D. Allen and H. F. Schaefer X, *J. Phys. Chem. A*, 2000, **104**, 9823.
35 M. J. Frisch, G. W. Trucks, H. B. Schlegel, G. E. Scuseria, M. A. Robb, J. R. Cheeseman, G. Scalmani, V. Barone, B. Mennucci, G. A. Petersson, H. Nakatsuji, M. Caricato, X. Li, H. P. Hratchian, A. F. Izmaylov, J. Bloino, G. Zheng, J. L. Sonnenberg, M. Hada, M. Ehara, K. Toyota, R. Fukuda, J. Hasegawa, M. Ishida, T. Nakajima, Y. Honda, O. Kitao, H. Nakai, T. Vreven, J. A. Montgomery Jr, J. E. Peralta, F. Ogliaro, M. Bearpark, J. J. Heyd, E. Brothers, K. N. Kudin, V. N. Staroverov, R. Kobayashi, J. Normand, K. Raghavachari, A. Rendell, J. C. Burant, S. S. Iyengar, J. Tomasi, M. Cossi, N. Rega, J. M. Millam, M. Klene, J. E. Knox, J. B. Cross, V. Bakken, C. Adamo, J. Jaramillo, R. Gomperts, R. E. Stratmann, O. Yazyev, A. J. Austin, R. Cammi, C. Pomelli, J. W. Ochterski, R. L. Martin, K. Morokuma, V. G. Zakrzewski, G. A. Voth, P. Salvador, J. J. Dannenberg, S. Dapprich, A. D. Daniels, O. Farkas, J. B. Foresman, J. V. Ortiz, J. Cioslowski, D. J. Fox, Gaussian, Inc, Wallingford CT, 2009.
36 S. E. Stein and B. S. Rabinovitch, *J. Chem. Phys.*, 1973, **58**, 2438–2445.
37 D. C. Astholz, J. Troe and W. Wieters, *J. Chem. Phys.*, 1979, **70**, 5107–5116.
38 NIST Computational Chemistry Comparison and Benchmark Database, http://srdata.nist.gov/cccbdb/.
39 Y. Z. Tang, H. F. Sun, J. Zhao, J. H. Liu and R. S. Wang, *Atmos. Environ.*, 2013, **65**, 164–170.
40 Y. Z. Tang, H. F. Sun, J. Y. Sun, Y. J. Zhang and R. S. Wang, *Atmos. Environ.*, 2014, **92**, 367–375.
41 C. T. Chang, T. H. Liu and F. T. Jeng, *Environ. Res.*, 2004, **94**, 67–74.
42 J. G. Anderson, *Geophys. Res. Lett.*, 1976, **3**, 165–168.
43 A. M. Kosmas and E. Drougas, *Chem. Phys.*, 2009, **358**, 230–234.

